PAPER

Check for updates

Hydrothermal synthesis, structures, and catalytic performance of five coordination compounds driven by 5-aminoisophthalic acid†

Zhen-Zhong Mei, Hong-Yu Wang, Chao Ren, Ying Yang [ID] and Jin-Zhong Gu [ID] *

An amino-functionalized-dicarboxylic acid, 5-aminoisophthalic acid (H_2aipa), was used as a versatile building block to synthesize a series of five novel coordination compounds under hydrothermal conditions and formulated as $[Co(\mu_3\text{-aipa})(2,2'\text{-}H_2biim)]_n$ (1), $[Ni_2(\mu\text{-aipa})_2(2,2'\text{-}H_2biim)_2(H_2O)_4] \cdot 4H_2O$ (2), $\{[Cd(\mu_3\text{-aipa})(2,2'\text{-}H_2biim)] \cdot H_2O\}_n$ (3), $\{[Ni(\mu\text{-aipa})(\mu\text{-bpb})] \cdot 0.5bpb \cdot H_2O\}_n$ (4), and $\{[Ni_2(\mu\text{-aipa})(\mu_3\text{-aipa})(\mu\text{-dpea})_2(H_2O)][Ni(\mu\text{-aipa})(\mu\text{-dpea})(H_2O)] \cdot 8H_2O\}_n$ (5). Three supporting ligands (2,2′-biimidazole (H_2biim),1,4-bis(pyrid-4-yl)benzene (bpb), and 1,2-di(4-pyridyl)ethane (dpea)) were used in the synthesis. The structures of the studied products **1–5** vary significantly, ranging from a 0D dimer (**2**), 2D sheets (**1**, **3** and **4**) to 3D + 2D interpenetrated frameworks (**5**). Furthermore, these compounds were evaluated as heterogeneous catalysts for the Knoevenagel reaction, achieving high product yields under optimized conditions. In addition, we also investigated various reaction parameters, substrate scope, and assessed the feasibility of catalyst recycling. This thorough investigation highlights the versatility of H_2aipa as a dicarboxylate building block in the formation of functional coordination polymers.
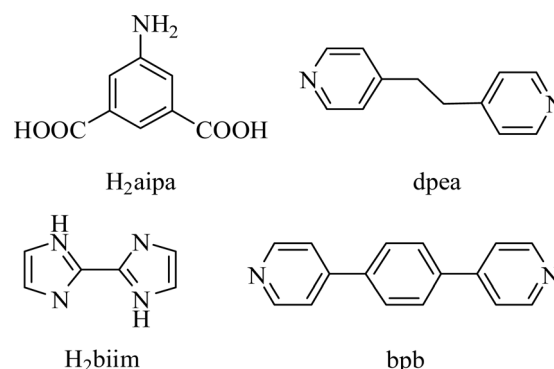
Introduction

Coordination polymers (CPs) are an important class of crystal materials that are constructed using self-assembly of metal ions with organic bridging ligands.[1–3] Their versatile topologies and chemical properties[4,5] make them ideal candidates for diverse applications such as gas adsorption and separation,[6–9] heterogeneous catalysis,[10–12] sensing,[8,13,14] and biomaterials.[15] To study the process of mineral formation under supercritical conditions in the laboratory, researchers initially employed hydrothermal and solvothermal synthesis methods. These days, hydrothermal synthesis is extensively utilized in the construction of CPs, especially for the preparation of CPs crystals.[16–19] The self-assembly in these reactions is highly sensitive to several variables including the types of metal ion, the concentration of reactants as well as the pH value of the solution.[20–23] Poly-carboxylate ligands are commonly used as versatile organic linkers in the synthesis of metal clusters and polymers.[24,25] This preference stems from their partially or fully deprotonated sites, which enable the development of different structural topologies and exhibit a variety of coordination modalities.[26] These

ligands, in particular, can function as terminal unidentate, chelating, bridging bidentate and bridging tridentate ligands.[27]

During the last few years, our research has focused on designing new functional coordination polymers using poly-carboxylic ligands.[10,18,28] In this study, we chose 5-amino-isophthalic acid (H_2aipa, Scheme 1) as a amino-functionalized dicarboxylate building block.

H_2aipa exhibits several intriguing properties that make it an attractive linker: (a) H_2aipa has five coordination sites, including one amino nitrogen and four carboxyl oxygen atoms. (b) The free amino nitrogen atom can act as a base site for catalysis, facilitating reactions such as the Henry reaction, cyanosilylation and Knoevenagel condensation.[28–30]

College of Chemistry and Chemical Engineering, Lanzhou University, Lanzhou 730000, People's Republic of China. E-mail: gujzh@lzu.edu.cn

† Electronic supplementary information (ESI) available: optical images (Fig. S1), FTIR spectra (Fig. S2), PXRD patterns (Fig. S3), additional catalysis data (Fig. S4–S7) and structural parameters (Tables S1 and S2). CCDC 2367606–2367610. For ESI and crystallographic data in CIF or other electronic format see DOI: https://doi.org/10.1039/d4ra05352d

Scheme 1 Structures of H_2aipa block and auxiliary ligands.

Here, we report the synthesis and characterization of five novel coordination compounds derived from metal(II) salts, H_2aipa, and three auxiliary ligands. These compounds exhibit diverse structures, ranging from a 0D dimer (2), 2D sheets (1, 3 and 4) to 3D + 2D interpenetrated frameworks (5), specifically $[Co(\mu_3\text{-aipa})(2,2'\text{-}H_2biim)]_n$ (1), $[Ni_2(\mu\text{-aipa})_2(2,2'\text{-}H_2biim)_2(H_2O)_4]\cdot4H_2O$ (2), $\{[Cd(\mu_3\text{-aipa})(2,2'\text{-}H_2biim)]\cdot H_2O\}_n$ (3), $\{[Ni(\mu\text{-aipa})(\mu\text{-bpb})]\cdot0.5bpb\cdot H_2O\}_n$ (4), and $\{[Ni_2(\mu\text{-aipa})(\mu_3\text{-aipa})(\mu\text{-dpea})_2(H_2O)][Ni(\mu\text{-aipa})(\mu\text{-dpea})(H_2O)]\cdot8H_2O\}_n$ (5).

In addition, we have also evaluated the catalytic activities of these compounds in the Knoevenagel reaction between pyridine-3-aldehyde with propanedinitrile.

Experimental section

General methods

All chemicals were purchased commercially utilized exactly as supplied. To record the FTIR spectra (KBr discs), a Bruker EQUINOX 55 spectrometer was utilized. Elemental analyses (EA) for carbon, hydrogen, and nitrogen in compounds 1–5 were conducted using an ElementarVario EL elemental analyzer. Thermogravimetric analyses (TGA) were conducted using a LINSEIS STA PT1600 thermal analyzer under a nitrogen flow and heating at a rate of 10 °C min^{-1}. The powder X-ray diffraction patterns (PXRD) of the compounds were collected using a Rigaku-Dmax 2400 diffractometer (CuKα radiation; $\lambda = 1.54060$ Å, Rigaku Corporation, Tokyo, Japan). For ^1H NMR experiments, a JNM ECS 400 M spectrometer was used with $CDCl_3$ as the solvent.

Synthesis of $[Co(\mu_3\text{-aipa})(2,2'\text{-}H_2biim)]_n$ (1)

A 20 mL Teflon cup was sealed with the following contents: H_2aipa (36.2 mg, 0.2 mmol), H_2biim (26.8 mg, 0.2 mmol), $CoCl_2\cdot6H_2O$ (47.6 mg, 0.2 mmol), NaOH (16.0 mg, 0.4 mmol), and H_2O (10 mL). After three days of heating the mixture at 160 °C, it was allowed to cool to ambient temperature. Purple block-shaped crystals were extracted and rinsed with water. Yield: 43% based on H_2aipa. Computed for $C_{14}H_{11}CoN_5O_4$: C 45.18, N 18.82, H 2.98%. Found: C 45.43, N 18.49, H 3.00%. FTIR (KBr, cm^{-1}): 3578 w, 3309 w, 1620 w, 1595 m, 1517 m, 1412 s, 1327 s, 1244 w, 1100 w, 1058 w, 995 w, 961 w, 920 w, 845 w, 778 m, 730 w, 666 w, 621 w 580 w, 547 w.

Synthesis of $[Ni_2(\mu\text{-aipa})_2(2,2'\text{-}H_2biim)_2(H_2O)_4]\cdot4H_2O$ (2)

Compound 2 was synthesized using a method analogous to CP 1 by substituting $NiCl_2\cdot6H_2O$ (47.6 mg, 0.2 mmol) for $CoCl_2\cdot6H_2O$. The synthesis yielded green block-shaped crystals of compound 2, with a 42% yield based on H_2aipa. Computed for $C_{28}H_{38}Ni_2N_{10}O_{16}$: C 37.87, N 15.77, H 4.31%. Found: C 38.03, N 15.85, H 4.28%. FTIR (KBr, cm^{-1}): 3273 m, 3168 w, 3120 w, 1617 w, 1554 s, 1487 w, 1371 s, 1270 w, 1192 w, 1128 w, 1054 w, 991 w, 964 w, 924 w, 864 w, 818 w, 785 m, 748 w, 715 m, 610 w, 570 w.

Synthesis of $\{[Cd(\mu_3\text{-aipa})(2,2'\text{-}H_2biim)]\cdot H_2O\}_n$ (3)

CP 3 was synthesized using a method analogous to CP 1 by substituting $CdCl_2\cdot H_2O$ (40.2 mg, 0.2 mmol) for $CoCl_2\cdot6H_2O$.

The synthesis yielded yellow block-shaped crystals of CP 3, with a 45% yield based on H_2aipa. Computed for $C_{14}H_{13}CdN_5O_5$: C 37.90, N 15.78, H 2.95%. Found: C 38.15, N 16.01, H 2.96%. FTIR (KBr, cm^{-1}): 3304 m, 3266 m, 3180 w, 1613 w, 1580 m, 1546 s, 1397 s, 1349 s, 1323 s, 1252 w, 1114 m, 1021 w, 964 w, 920 w, 853 w, 782 m, 734 w, 673 w, 595 w, 540 w.

Synthesis of $\{[Ni(\mu\text{-aipa})(\mu\text{-bpb})]\cdot0.5bpb\cdot H_2O\}_n$ (4)

A 20 mL Teflon cup was sealed with the following contents: H_2aipa (36.2 mg, 0.2 mmol), bpb (46.4 mg, 0.2 mmol), $NiCl_2\cdot6H_2O$ (47.6 mg, 0.2 mmol), NaOH (16.0 mg, 0.4 mmol), and H_2O (10 mL). After three days of heating the mixture at 160 °C, it was allowed to cool to ambient temperature. Green block-shaped crystals were extracted and rinsed with water. Yield: 46% based on H_2aipa. Computed for $C_{32}H_{25}N_4NiO_5$: C 63.61, N 9.27, H 4.17%. Found: C 63.90, N 9.23, H 4.20%. FTIR (KBr, cm^{-1}): 3359 m, 3309 m, 3083 w, 1614 s, 1546 s, 1480 w, 1386 s, 1226 w, 1110 w, 1073 w, 1013 w, 905 w, 804 m, 726 w, 678 w, 618 w, 573 w.

Synthesis of $\{[Ni_2(\mu\text{-aipa})(\mu_3\text{-aipa})(\mu\text{-dpea})_2(H_2O)][Ni(\mu\text{-aipa})(\mu\text{-dpea})(H_2O)]\cdot8H_2O\}_n$ (5)

A 20 mL Teflon cup was sealed with the following contents: H_2aipa (36.2 mg, 0.2 mmol), dpea (36.8 mg, 0.2 mmol), $NiCl_2\cdot6H_2O$ (47.6 mg, 0.2 mmol), NaOH (16.0 mg, 0.4 mmol), and H_2O (10 mL). After three days of heating the mixture at 160 °C, it was allowed to cool to ambient temperature. Green block-shaped crystals were extracted and rinsed with water. Yield: 43% based on H_2aipa. Computed for $C_{60}H_{71}N_9Ni_3O_{22}$: C 49.83, N 8.72, H 4.95%. Found: C 50.17, N 8.75, H 4.91%. FTIR (KBr, cm^{-1}): 3445 w, 3363 m, 3236 w, 1621 m, 1546 s, 1468 w, 1431 m, 1382 s, 1222 w, 1099 w, 1069 w, 1024 w, 957 w, 894 w, 831 w, 789 m, 726 m, 673 w, 606 w, 547 w.

Single crystal X-ray diffraction & topological analysis

A Bruker APEX-II CCD diffractometer was used to collect the crystal data of compounds 1–5 using graphite-monochromated Mo/CuK$_\alpha$ radiation; $\lambda = 0.71073/1.54178$ Å). SHELXS-97 and SHELXL-97 software were used for the determination of the structures.[31] Detailed crystal parameters and structural refinements can be found in Table 1, with selected bond parameters are listed in Tables S1 and S2 (ESI).† The supplementary crystallographic data for compounds 1–5 are available in CCDC 2367606–2367610.

Topological analysis of the obtained coordination polymers was conducted using ToposPro software. This involved generating a simplified underlying net, wherein bridging ligands were reduced to the centroids.[32,33]

Catalytic activity in Knoevenagel reaction

The following ingredients were mixed in a suspension and stirred at 25 °C for a required reaction time: catalyst (2.0 mol%), aromatic aldehyde (0.50 mmol), propanedinitrile (1.0 mmol), and solvent (1.0 mL, usually CH_3OH). Centrifugation was subsequently used to extract the catalyst. A crude solid product

Table 1 Crystal data for **1–5**

Compound	1	2	3	4	5
Chemical formula	$C_{14}H_{11}CoN_5O$	$C_{28}H_{38}Ni_2N_{10}O_{16}$	$C_{14}H_{13}CdN_5O_5$	$C_{32}H_{25}N_4NiO_5$	$C_{60}H_{71}N_9Ni_3O_{22}$
Formula weight	372.21	888.10	443.68	604.27	1446.24
Crystal system	Triclinic	Monoclinic	Triclinic	Monoclinic	Triclinic
Space group	$P\bar{1}$	$P2_1/c$	$P\bar{1}$	$P2_1/n$	$P1$
a/Å	7.6951(3)	11.9238(3)	7.89650(10)	11.0968(4)	10.1262(3)
b/Å	8.0250(2)	8.0959(2)	8.16800(10)	22.3594(7)	13.2389(3)
c/Å	11.2161(6)	18.3412(5)	11.4250(2)	11.6156(4)	13.3575(3)
α/°	83.335(3)	90	83.7430(10)	90	88.8838(17)
β/°	76.981(4)	95.998(2)	77.408(2)	107.065(4)	75.6606(19)
γ/°	81.112(3)	90	81.2660(10)	90	74.270(2)
V Å^{-3}	664.34(5)	1760.85(8)	708.630(19)	2755.14(18)	1667.75(7)
T/K	303(2)	303(2)	285(2)	293(2)	303(2)
Z	2	2	2	4	1
D_c/g cm^{-3}	1.861	1.675	1.995	1.457	1.297
μ/mm^{-1}	1.326	1.159	12.657	0.754	1.530
$F(000)$	378	920	420	1252	674
Refl. measured	2470	3277	2577	5127	8599
Unique refl. (R_{int})	2264 (0.0319)	2914 (0.0332)	2463 (0.0291)	4389 (0.0261)	8204 (0.0380)
GOF on F^2	1.136	1.031	1.037	1.051	1.066
$R_1[I > 2\sigma(I)]^a$	0.0369	0.0324	0.0226	0.0300	0.0420
$wR_2[I > 2\sigma(I)]^b$	0.0759	0.0864	0.0579	0.0788	0.1184

^{a} $R_1 = \Sigma||F_o| - |F_c||/|F_o|$. ^{b} $wR_2 = \{\Sigma[w(F_o{}^2 - F_c{}^2)]^2/\Sigma[w(F_o{}^2)]^2\}^{1/2}$.

was obtained by evaporating the filtrate using a rotary evaporator. The amount of this solid product was ascertained by ^{1}H NMR spectroscopy (JNM ECS 400M spectrometer) after it was dissolved in CDCl$_3$ (Fig. S7, ESI†). The catalyst was recovered by centrifugation, washed with methanol, allowed to dry at room temperature, and subsequently reused in further reactions, following the same procedure for recycling experiments.

Results and discussion

Hydrothermal synthesis of compounds 1–5

A series of reactions were conducted under hydrothermal conditions to assess the potential of 5-aminoisophthalic acid (H$_2$aipa) as a building block for synthesizing coordination polymers. These reactions involved a mixture of metal(II) salts, H$_2$aipa, sodium hydroxide, and an auxiliary ligand selected from the following H$_2$biim, bpb, and dpea. The hydrothermal synthesis was carried out at 160 °C for three days, followed by

a gradual reduction in temperature to promote the crystallization of CPs. The resulting products were collected in substantial yields and analyzed using standard techniques. The synthesis repeatability of the five complexes is good and the yields are stable. The experimental PXRD patterns of products **1–5** agree with the computed diffractograms (Fig. S3†), suggesting their homogeneous phase purity. Structural discrepancies among compounds **1–5** could be attributed to the varying auxiliary ligands and the coordination properties of the metal(II) centers.

Description of structures

[Co(μ$_3$-aipa)(2,2′-H$_2$biim)]$_n$ (1). The asymmetric unit of CP **1** contains a μ$_3$-aipa^{2-} block, a Co(II) center, and a H$_2$biim auxiliary ligand (Fig. 1a). The Co1 center is six-coordinate with the Co1 center being coordinated by three carboxyl oxygen and one N atoms from three μ$_3$-aipa^{2-} linkers and two N donors from the H$_2$biim moiety and forms a distorted octahedral {CoN$_3$O$_3$} geometry. The Co–O and Co–N bond lengths, which
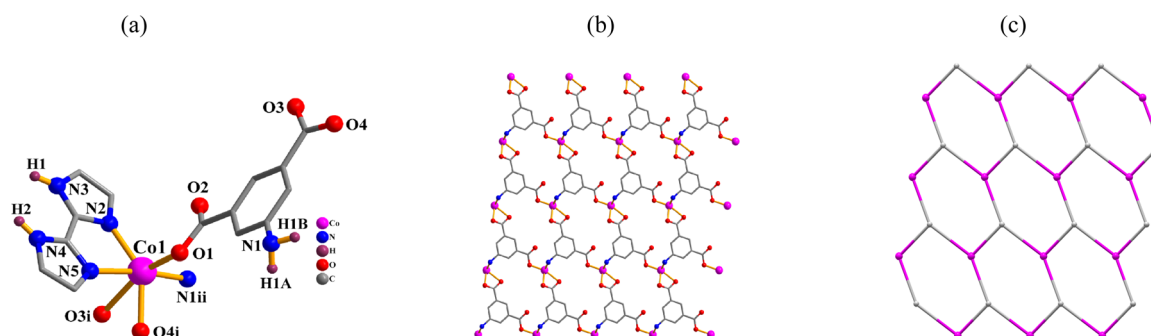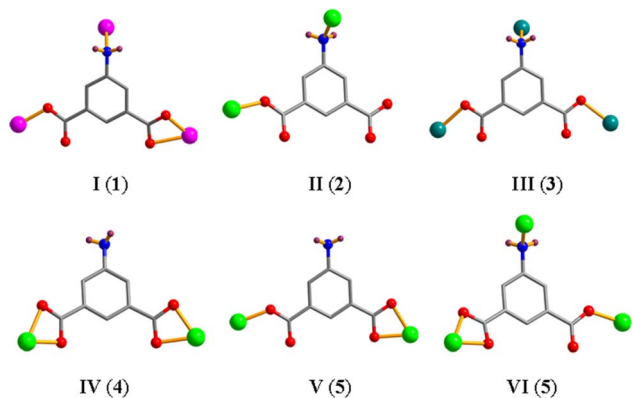

Fig. 1 Structure of CP **1**. (a) Coordination environment at cobalt(II) atom. (b) The two-dimensional layer viewed along the c axis. (c) The sheet exhibiting a **hcb** topology, observed along the c axis.

Scheme 2 The coordination modes of aipa^{2-}.

measure 2.044(2)–2.399(2) and 2.087(2)–2.230(3) Å, are within the typical ranges for Co(II) compounds.[18,28] In CP **1**, the aipa^{2-} ligand exhibits the coordination mode I (Scheme 2) with two monodentate or bidentate COO$^-$ groups. Furthermore, the nitrogen atom of the NH$_2$ is involved in coordination. The μ$_3$-aipa^{2-} blocks connect the Co(II) centers, forming a 2D sheet (Fig. 1b) with **hcb** topology (Fig. 1c).

[Ni$_2$(μ-aipa)$_2$(2,2′-H$_2$biim)$_2$(H$_2$O)$_4$]·4H$_2$O (2). One Ni(II) atom, one μ-aipa^{2-} block, one H$_2$biim, two H$_2$O ligands and two lattice water molecules form the asymmetric unit of compound **2** (Fig. 2a). The six-coordinate Ni1 atom shows a distorted

octahedral {NiN$_3$O$_3$} environment. It comprises one carboxyl oxygen and one N atoms from two μ-aipa^{2-} blocks, two O donors from two H$_2$O ligands, and a pair of N atoms of a H$_2$biim moiety. The Ni–O [2.021(2)–2.120(2) Å] and Ni–N [2.072(2)–2.164(2) Å] bond lengths fall within the expected ranges.[18,28] The cpic^{2-} block functions as a μ-linker (mode II, Scheme 2). Fig. 2b shows that a Ni$_2$ molecule is formed when two μ-aipa^{2-} blocks link two Ni1 atoms. These Ni$_2$ molecules are further assembled into a 3D H-bonded supramolecule framework (Fig. 2c).

{[Cd(μ$_3$-aipa)(2,2′-H$_2$biim)]·H$_2$O}$_n$ (3). CP **3** is an asymmetric unit with one μ$_3$-aipa^{2-} block, one cadmium(II) center, one H$_2$biim supporting ligand, and one lattice water molecule. The five-coordinate Cd1 atom has a distorted trigonal bipyramidal {CdO$_2$N$_3$} geometry (Fig. 3a), made up of one nitrogen and two carboxyl oxygen atoms from three distinct μ$_3$-aipa^{2-} blocks and two Ndonor from the H$_2$biim ligand. The Cd–O [2.248(2)–2.285(2) Å] and Cd–N [2.257(2)–2.447(3) Å] distances are comparable to those in Cd(II) derivatives.[28,29] In **3**, the aipa^{2-} block behaves as a μ$_3$-spacer (mode III, Scheme 2). The adjacent cadmium(II) atoms are linked by μ$_3$-aipa^{2-} blocks, generating a 2D sheet (Fig. 3b) with a **hcb** topology (Fig. 3c).

{[Ni(μ-aipa)(μ-bpb)]·0.5bpb·H$_2$O}$_n$ (4). CP **4** is an asymmetric unit with one Ni(II) center, one μ-aipa^{2-} block, a half of μ-bpb, moiety and one free water molecule. The compound forms a two-dimensional coordination polymer (Fig. 4a). As shown in Fig. 4a, the nickel center is six-coordinate and form a distorted octahedral {NiO$_4$N$_2$} geometry. The geometry is completed by
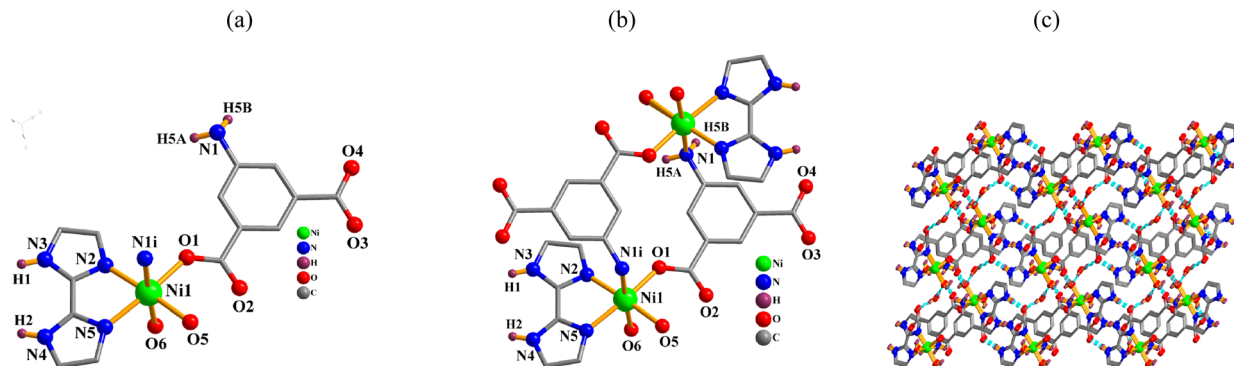

Fig. 2 Structure of dimer **2**. (a) Coordination environment at nickel(II) atom. (b) The Ni$_2$ molecule. (c) A 3D H-bonded supramolecule framework; view along the *b* axis.
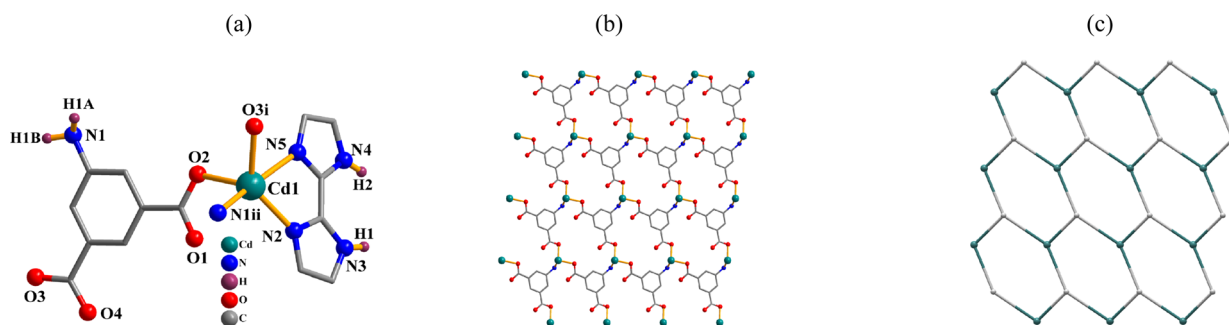

Fig. 3 Structure of CP **3**. (a) Coordination environment at cadmium(II) center. (b) The two-dimensional layer viewed along the *c* axis. (c) Sheet exhibiting a **hcb** topology, observed along the *c* axis.
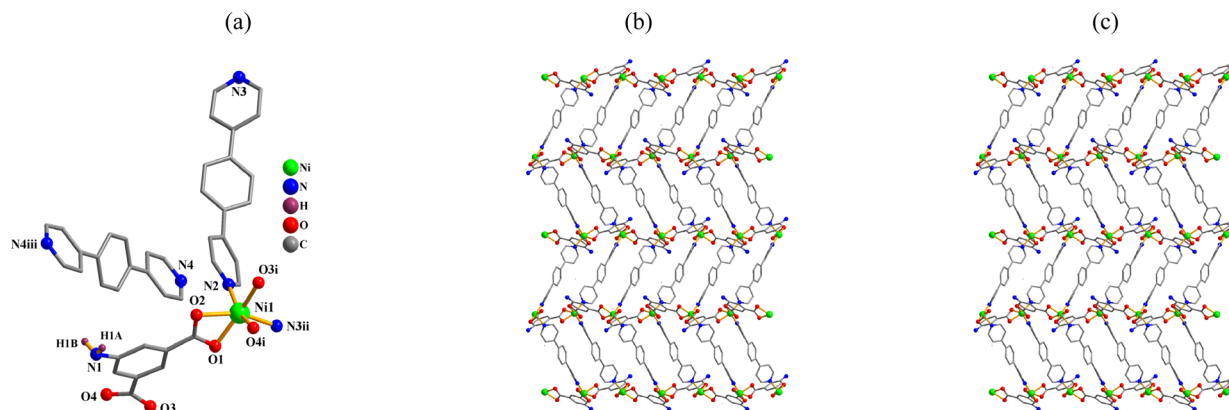
Fig. 4 Structure of **4**. (a) Coordination environment at the nickel(II) atom. (b) The two-dimensional layer viewed along the *a* axis. (c) Sheet exhibiting a **new** topology, viewed along the *a* axis.

two N_{bpb} atoms from two μ-bpb moieties and four carboxyl oxygen atoms from two μ-aipa^{2-}. The Ni–O [2.052(2)–2.192(2) Å] and Ni–N [2.050(2)–2.062(2) Å] bond lengths fall within expected ranges.[18,28] The aipa^{2-} moiety adopts μ-coordination fashion (mode IV, Scheme 2). The aipa^{2-} and bpb ligands linked neighbouring Ni(II) centers, resulting a 2D layer (Fig. 4b) with a **new** topology and point symbol of $(8^4.12^2)(8)_2$ (Fig. 4c).

{[Ni$_2$(μ-aipa)(μ$_3$-aipa)(μ-dpea)$_2$(H$_2$O)][Ni(μ-aipa)(μ-dpea)(H$_2$-O)]·8H$_2$O}$_n$ (5). The structure consists of a [Ni(μ-aipa)(μ-dpea)(H$_2$O)]$_n$ 2D sheet and a [Ni$_2$(μ-aipa)(μ$_3$-aipa)(μ-dpea)$_2$(H$_2$-O)]$_n$ 3D framework. CP **5** is an asymmetric unit with three

distinct nickel(II) centers, three aipa^{2-} blocks, three dpea, two coordinated water molecules, and eight lattice water molecules. The Ni1 and Ni3 atoms exhibit distorted octahedral {NiO$_4$N$_2$} coordination geometries, which include three carboxyl oxygen atoms from two distinct aipa^{2-} blocks, one O atom from the H$_2$O ligand, and two N donors from two dpea ligands (Fig. 5a). The six-coordinate nickel 2 center forms a distorted octahedral {NiO$_3$N$_3$} configuration. It is surrounded by one nitrogen and three oxygen atoms from three distinct aipa^{2-} blocks, as well as two N atoms of two dpea ligands. The Ni–O [2.002(3)–2.158(4) Å] and Ni–N [2.070(4)–2.145(4) Å] bond lengths are similar to those
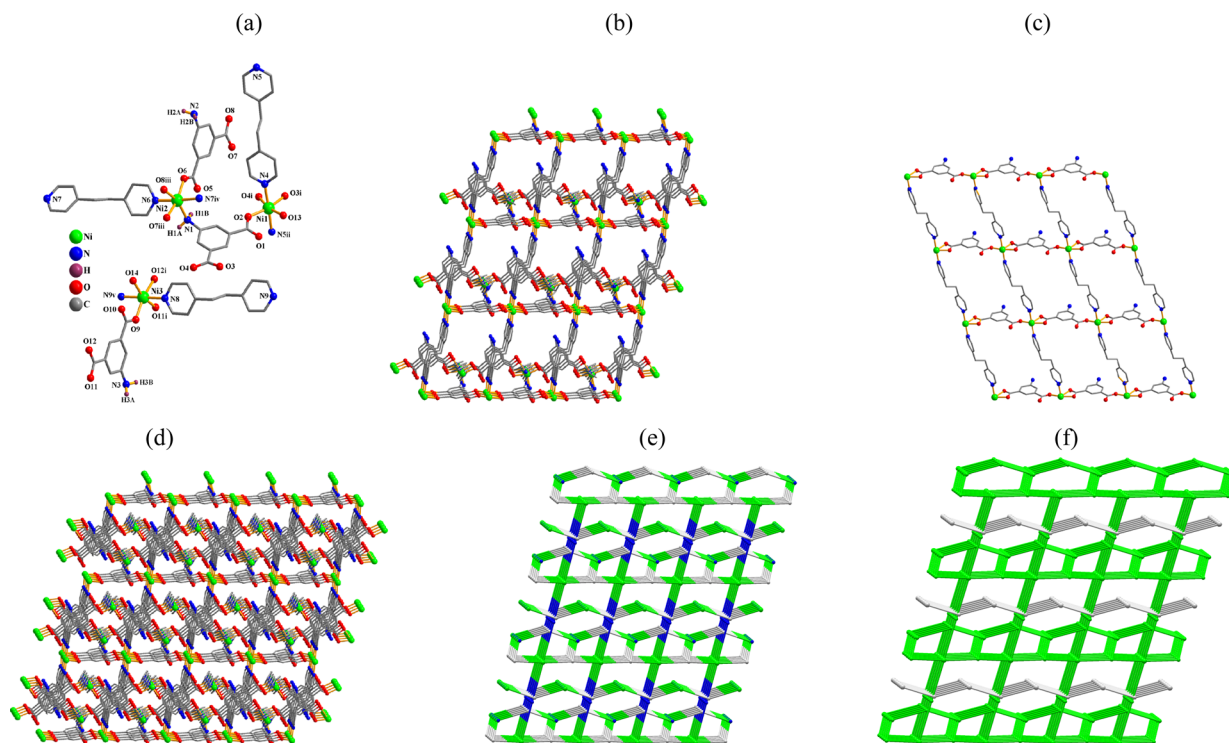

Fig. 5 Structure of 5. (a) Coordination environment at nickel(II) atoms. (b) Three-dimensional framework along the *c* axis. (c) Two-dimensional metal–organic network along the *b* axis. (d) 3D + 2D interpenetrated frameworks along the *c* axis. (e) Topological representation of the framework along the *c* axis. (f) Two 3D + 2D interpenetrated frameworks shown by different colours (green and gray).

observed in analogous Ni(II) derivatives.[18,28] The aipa^{2-} blocks act as μ- or μ$_3$-linkers (modes IV and V, Scheme 2). The dpea shows a bridging coordination fashion. The μ-aipa, μ$_3$-aipa and μ-dpea blocks linked Ni1 and Ni2 centers to form a 3D framework (Fig. 5b). Meanwhile, the Ni3 atoms were connected by the μ$_3$-aipa and μ-dpea ligands to generate a 2D layer (Fig. 5c). Finally, 3D + 2D interpenetrated frameworks were formed (Fig. 5d) with a **new** topology and point symbol of $(8^4 \cdot 12^2)(8)_2$ (Fig. 5e and f).

TGA & PXRD data

The assessment of thermal stability for compounds **1–5** was carried out using thermogravimetric analysis (TGA) under a N$_2$ atmosphere within a temperature range of 23–800 °C (Fig. 6). The CP **1** does not contain coordinated or crystallization water, so its network is stable up to 395 °C. At temperatures 72 to 292 °C, dimer **2** lost four lattice and four coordinated water molecules (exptl 15.9%; calculated 16.2%), whereas the dehydrated sample held steady until 316 °C. For CP **3**, a weight loss of 4.3% (calcd 4.1%) occurred at temperatures from 28 and 193 °C, associated with the release of one lattice water molecule. In CP **4**, one lattice water and a half of bpb were lost at 28–193 °C (exptl, 22.0%; calcd, 22.2%), with the dehydrated sample is stable up to 343 °C. For CP **5**, a mass loss between 29–190 °C indicated the release of eight lattice water molecules and two coordinated water molecules (exptl 12.1%, calculated 12.4%), whereas the sample held steady until 335 °C.

Power X-ray diffractograms were acquired at 25 °C for compounds **1–5** (Fig. S3†). Phase purity of all samples was established by analyzing the experimental patterns and comparing them with the simulated ones (based on CIF data).

Catalytic Knoevenagel reaction

We investigated compounds **1–5** for their potential as heterogeneous catalysts in the Knoevenagel reaction, which involves a combination of propanedinitrile and a variety of aldehydes, considering the possibility of different coordination complexes acting as catalysts in this reaction.[28–30,34,35] Using pyridine-3-aldehyde as a model substrate, we reacted it with
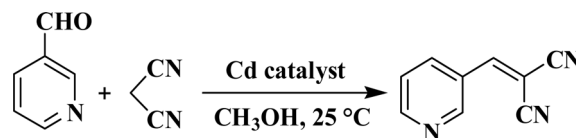
Scheme 3 Knoevenagel reaction of pyridine-3-aldehyde with propanedinitrile.

malononitrile at 25 °C in methanol to synthesize the related product. As a model substrate, pyridine-3-aldehyde was reacted with malononitrile at 25 °C methanol (Scheme 3 and Table 2). Furthermore, we conducted a thorough investigation of various reaction parameters, which included the duration of the reaction, the type of solvent used, catalyst loading, potential for catalyst reuse, and the scope of substrates involved. CP **3** exhibited the highest activity, achieving a >99 conversion rate of pyridine-3-aldehyde (Table 2). It was then used to study the effects of different reaction parameters. The yield increased from 55 to >99% when the reaction time was extended from 10 to 60 min (Table 2, entries 1–6). The impact of catalyst amount was also examined, and the results showed that increasing the loading of catalyst from 1 to 2 mol% increased product yield from 95 to >99% (entries 6 and 11). It is worth mentioning that various solvents, including methanol, were tested in these reactions. Chloroform, acetonitrile, water, and ethanol all have lower product yields (66–98% product yields). Compounds **1**, **2**, **4** and **5** exhibit reduced activity when compared to CP **3**, achieving product yields in the 82–90% range (entries 12–15, Table 2). It is worth mentioning that the Knoevenagel reaction of pyridine-3-aldehyde is much less efficient without a catalyst (only 20% product yield) or when H$_2$aipa or CdCl$_2$ are used as catalysts (28% yield or 24% yield), respectively under comparable reaction conditions (entries 16–18, Table 2). The improved performance of CP **3** is likely due to the presence of unsaturated coordination sites in the Cd(II) centers, which makes it easier to access the substrates.[28,30,32]

A range of substituted benzaldehyde substrates was evaluated to determine the substrate scope in the Knoevenagel reaction with propanedinitrile. These reactions were carried out under optimized conditions (2.0 mol% **3**, methanol, 25 °C, 1 h). Table 3 shows that the yields of the respective products ranged from 33 to >99%. Benzaldehydes with strong electron-withdrawing groups, such as nitro, chloro, bromo and fluoro substituents, demonstrated the highest efficiency (entries 2–7, Table 3). This increased efficiency is likely due to the higher electrophilicity of these substrates. However, benzaldehydes with electron-donating groups, such as methyl or methoxy groups, resulted in lower product yields (entries 9 and 10, Table 3).

The recyclability of catalyst **3** was evaluated. After every reaction cycle, the catalyst was separated by centrifugation, rinsed inmethanol, air-dried at approximately 25 °C, and reused in the subsequent cycle. The data show that CP **3** retains its activity for at least five more reaction cycles (Fig. S5†). Additionally, PXRD patterns show that the structure of CP **3** remains intact (Fig. S6†), despite the occurrence of multiple new signals
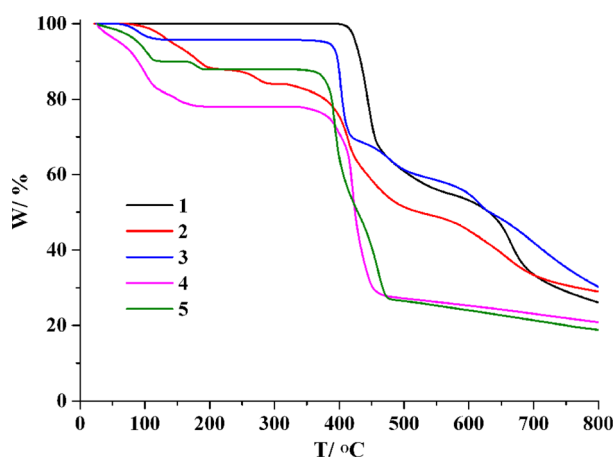
Fig. 6 TGA plots of **1–5**.

Table 2 Knoevenagel reaction of pyridine-3-aldehyde with propanedinitrile[a]

Entry	Catalyst	Reaction time (min)	Catalyst loading (mol%)	Solvent	Product yield[b] (%)
1	**3**	10	2.0	CH_3OH	55
2	**3**	20	2.0	CH_3OH	75
3	**3**	30	2.0	CH_3OH	84
4	**3**	40	2.0	CH_3OH	91
5	**3**	50	2.0	CH_3OH	96
6	**3**	60	2.0	CH_3OH	>99
7	**3**	60	2.0	H_2O	98
8	**3**	60	2.0	C_2H_5OH	96
9	**3**	60	2.0	CH_3CN	86
10	**3**	60	2.0	$CHCl_3$	66
11	**3**	60	1.0	CH_3OH	95
12	**1**	60	2.0	CH_3OH	82
13	**2**	60	2.0	CH_3OH	87
14	**4**	60	2.0	CH_3OH	85
15	**5**	60	2.0	CH_3OH	90
16	Blank	60	—	CH_3OH	20
17	$CdCl_2 \cdot 2H_2O$	60	2.0	CH_3OH	32
18	H_2aipa	60	2.0	CH_3OH	26

[a] Conditions: pyridine-3-aldehyde (0.5 mmol), propanedinitrile (1.0 mmol), catalyst (1–2 mol%), solvent (1.0 mL), 25 °C. [b] Yield based on ^{1}H NMR analysis: [moles of product per mol of aldehyde substrate] × 100%.

Table 3 Substrate scope for Cd-catalyzed Knoevenagel reaction of substituted benzaldehydes with propanedinitrile[a]

Entry	Substituted benzaldehyde	Product yield[b] (%)
1	Benzaldehyde	>99
2	2-Nitrobenzaldehyde	>99
3	3-Nitrobenzaldehyde	>99
4	4-Nitrobenzaldehyde	>99
5	4-Chlorobenzaldehyde	>99
6	4-Bromobenzaldehyde	>99
7	4-Fluorobenzaldehyde	>99
8	Pyridine-4-aldehyde	>99
9	4-Methylbenzaldehyde	97
10	4-Methoxybenzaldehyde	66
11	4-Hydroxybenzaldehyde	33

[a] Conditions: aldehyde (0.5 mmol), propanedinitrile (1.0 mmol), catalyst **3** (2.0 mol%), CH_3OH (1.0 mL), 25 °C. [b] Yield on the basis of ^{1}H NMR analysis: [moles of product per mol of aldehyde substrate] × 100%.

or widened peaks. These changes are likely due to the existence of certain or a decrease in crystallinity after multiple catalytic cycles.

Referring to previous studies in this area,[36–40] we propose a possible reaction mechanism for the Knoevenagel condensation catalyzed by **3** (Scheme S1, ESI†). The unsaturated Cd(II) metal centers of the catalyst (5-coordinate cadmium centers) eventually act as the Lewis acid sites interacting with the H–C=O functionality of pyridine-3-aldehyde, leading to its polarization and an enhanced electrophilicity of the corresponding carbon atom. Such a polarization can facilitate a nucleophilic attack of this site by propanedinitrile acting as a nucleophile precursor. On the other hand, an interaction between the Lewis acid site and the –CN group of malononitrile

augments an acidic character of the methylene functionality and enhances its deprotonation. The basic sites present in **3** (O-carboxylate sites) can easily abstract H$^+$ from the –CH$_2$– group to give rise to a nucleophile that would attack the H–C=O moiety of pyridine-3-aldehyde and result in the C–C bond formation, followed by the dehydration to give the 2-(pyridin-3-ylmethylene)malononitrile product.

Conclusions

This study showed the use of H_2aipa as a amino-functionalized dicarboxylate precursor to synthesize five novel coordination compounds using a hydrothermal method. These compounds **1–5** exhibit diverse structural features, ranging from 0D dimer (compound **2**), 2D sheets (CPs **1**, **3** and **4**) to 3D + 2D inter-penetrated frameworks (CP **5**). The catalytic potential of compounds **1–5** was evaluated in Knoevenagel reaction, which involved pyridine-3-aldehyde and propanedinitrile. CP **3** showed significant catalytic efficiency in this reaction.

Data availability

The data supporting this article have been included as part of the ESI.† CCDC-2367606–2367610 (compounds **1–5**) contain the supplementary crystallographic data for this paper.

Conflicts of interest

There are no conflicts to declare.

Acknowledgements

Notes and references

1 G. Chakraborty, I. H. Park, R. Medishetty and J. J. Vittal, *Chem. Rev.*, 2021, **121**, 3751–3891.

2 G. Maurin, C. Serre, A. Cooper and G. Ferey, *Chem. Soc. Rev.*, 2017, **46**, 3104–3107.

3 Z. J. Chen, K. O. Kirlikovali, P. Li and O. K. Farha, *Acc. Chem. Res.*, 2022, **55**, 579–591.

4 L. K. Macreadie, R. Babarao, C. J. Setter, S. J. Lee, O. T. Qazvini, A. J. Seeber, J. Tsanaktsidis, S. G. Telfer, S. R. Batten and M. R. Hill, *Angew. Chem., Int. Ed.*, 2020, **59**, 6090–6098.

5 X. Y. Dong, Y. Si, J. S. Yang, C. Zhang, Z. Han, P. Luo, Z. Y. Wang, S. Q. Zang and T. C. W. Mak, *Nat. Commun.*, 2020, **11**, 3678.

6 S. F. Gu, X. H. Xiong, L. L. Gong, H. P. Zhang, Y. Xu, X. F. Feng and F. Luo, *Inorg. Chem.*, 2021, **60**, 8211–8217.

7 L. Fan, Z. Liu, Y. Zhang, D. Zhao, J. Yang and X. Zhang, *Inorg. Chem. Commun.*, 2019, **107**, 107463.

8 D. Wu, J. Liu, J. Jin, J. Cheng, M. Wang, G. Yang and Y. Y. Wang, *Cryst. Growth Des.*, 2019, **19**, 6774–6783.

9 Y. Zhao, L. Wang, N. N. Fan, M. L. Han, G. P. Yang and L. F. Ma, *Cryst. Growth Des.*, 2018, **18**, 7114–7121.

10 X. Q. Kang, C. Ren, Z. Z. Mei, X. X. Fan, J. J. Xue, Y. L. Shao and J. Z. Gu, *Molecules*, 2023, **28**, 7474.

11 Y. Zheng, Q. Shen, Z. Li, X. Jing and C. Duan, *Inorg. Chem.*, 2022, **61**, 11156–11164.

12 D. Markad and S. K. Mandal, *Dalton Trans.*, 2018, **47**, 5928–5932.

13 M. Mörtel, J. Oschwald, A. Scheurer, T. Drewello and M. M. Khusniyarov, *Inorg. Chem.*, 2021, **60**, 14230–14237.

14 A. Rashid, S. Mondal and P. Ghosh, *Molecules*, 2023, **28**, 1231.

15 P. Q. Hung, P. Y. Lin, X. H. Wang and J. A. Ho, *J. Chin. Chem. Soc.*, 2023, **70**, 1284–1296.

16 Y. Qin, P. She, X. Huang, W. Huang and Q. Zhao, *Coord. Chem. Rev.*, 2020, **416**, 213331.

17 L. C. Hong, L. Y. Lin, L. Wei and K. Y. Fei, *Chin. J. Struct. Chem.*, 2021, **40**, 363–368.

18 X. Q. Kang, J. H. Wang and J. Z. Gu, *Chin. J. Inorg. Chem.*, 2023, **39**, 2385–2392.

19 R. S. Singh, R. P. Paitandi, R. K. Gupta and D. S. Pandey, *Coord. Chem. Rev.*, 2020, **414**, 213269.

20 S. Islam, S. Tripathi, A. Hossain, S. K. Seth and S. Mukhopadhyay, *J. Mol. Struct.*, 2022, **1265**, 133373.

21 D. Fonseca, A. F. Pérez-Torres, J. Cobo, J. Zapata-Rivera, J. J. Hurtado and M. A. Macías, *CrystEngComm*, 2022, **24**, 2982–2991.

22 M. Xu, G. Liang, S. Wang, X. Ma, G. Liang and Q. Ni, *J. Mol. Struct.*, 2020, **1217**, 128411.

23 J. J. Kong, D. Shao, J. C. Zhang, Y. X. Jiang, C. L. Ji and X. C. Huang, *CrystEngComm*, 2019, **21**, 749–757.

24 Q. P. Li and J. J. Qian, *RSC Adv.*, 2014, **4**, 32391–32397.

25 J. J. Qian, F. L. Jiang, K. Z. Su, J. Pan, L. J. Zhang, X. J. Li, D. Q. Yuan and M. C. Hong, *J. Mater. Chem. A*, 2013, **1**, 10631–10634.

26 R.-W. Huang, B. Li, Y.-Q. Zhang, Y. Zhao, S.-Q. Zang and H. Xu, *Inorg. Chem. Commun.*, 2014, **39**, 106–109.

27 X. Chai, H. Zhang, S. Zhang, Y. Cao and Y. Chen, *J. Solid State Chem.*, 2009, **182**, 1889–1898.

28 X. X. Fan, H. Y. Wang, J. Z. Gu, D. Y. Lv, B. Zhang, J. J. Xue, M. V. Kirillova and A. M. Kirillov, *Inorg. Chem.*, 2023, **62**, 17612–17624.

29 Z. W. Zhai, S. H. Yang, Y. R. Lv, C. X. Du, L. K. Li and S. Q. Zang, *Dalton Trans.*, 2019, **48**, 4007–4014.

30 Y. Q. Cai, Y. Q. Peng and G. H. Song, *Catal. Lett.*, 2006, **109**, 61–64.

31 G. M. Sheldrick, *SHELXS-97; Program for X-Ray Crystal Structure Determination*, University of Gottingen, Göttingen, Germany, 1997.

32 V. A. Blatov, *IUCrCompComm Newsletter*, 2006, vol. 7, pp. 4–38.

33 V. A. Blatov, A. P. Shevchenko and D. M. Proserpio, *Cryst. Growth Des.*, 2014, **14**, 3576–3586.

34 H. Chen, L. Fan, T. Hu and X. Zhang, *Inorg. Chem.*, 2021, **60**, 3384–3392.

35 M. Almasi, V. Zelenak, M. Opanasenko and J. Cejka, *Dalton Trans.*, 2014, **43**, 3730–3738.

36 N. Seal, A. Karmakar, P. P. Mondal, S. Kundu and S. Neogi, *ACS Appl. Mater. Interfaces*, 2024, **16**, 41721–41733.

37 B. Parmar, P. Patel, V. Murali, Y. Rachuri, R. I. Kureshy, N.-u. H. Khan and E. Suresh, *Inorg. Chem. Front.*, 2018, **5**, 2630–2640.

38 R. Pandey, D. Singh, N. Thakur and K. K. Raj, *ACS Omega*, 2021, **6**, 13240–13259.

39 M. Saghian, S. Dehghanpour and Z. bayatani, *Sci. Rep.*, 2023, **13**, 15563.

40 R. Chand, A. Karmakar, S. Kundu and S. Neogi, *Small*, 2024, 2404085.